Scale dependence of the Young modulus measured by nanoindentation in columnar YSZ EB-PVD thermal barriers coatings

Yves Gaillard, Emilio Jiménez-Piqué, Marc Anglada

Scale dependence of the Young modulus measured by nanoindentation in columnar YSZ EB-PVD thermal barriers coatings

Journal:	*Philosophical Magazine & Philosophical Magazine Letters*
Manuscript ID:	TPHM-05-Oct-0447.R1
Journal Selection:	Philosophical Magazine
Date Submitted by the Author:	06-Mar-2006
Complete List of Authors:	gaillard, yves; UPC, CMEM Jiménez-piqué, Emilio; UPC, CMEM anglada, marc; UPC, CMEM
Keywords:	AFM, thermal barrier coatings
Keywords (user supplied):	nanoindentation, EB-PVD

Scale dependence of the Young modulus measured by nanoindentation in columnar YSZ EB-PVD thermal barriers coatings

Y. GAILLARD, E. JIMENEZ-PIQUE and M. ANGLADA

Department of Materials Science and Metallurgy (CMEM), Universitat Politécnica de Catalunya, Avda. Diagonal 647 (ETSEIB), 08028 Barcelona, Spain.

Abstract :

Electron beam physical vapour deposited yttria stabilised zirconia (YSZ) thermal barrier coatings have been investigated by nanoindentation. It is shown that the mechanical properties, and particularly the Young modulus, of these coatings are closely related to their columnar microstructure. The transition from intra-columnar to inter-columnar deformation is characterised by a difference between the mechanical properties of the bulk YSZ and the ones of the coatings. The use of different indenter shape showed that the contact area was the parameter characteristic of this scale dependence. The deformation mechanisms studied by AFM have shown a good correlation with the evolution of the mechanical properties during the deformation.

Keywords : Thermal barrier coatings, nanoindentation, EB-PVD, AFM.

§ 1.Introduction :

Thermal barriers coatings (TBC) are widely used in the aircraft industry as protective coatings for gas engines turbine components. These tri-layered materials are composed

of an intermetallic bond coat (BC) deposited on a substrate, generally a super-alloy, and a ceramic top coat deposited on the bond coat. A thermally growth oxide (TGO) localised between the BC and the top coat is also formed during the deposition. The bond coat is an oxidation protection for the alloy while the top coat acts as the thermal insulator. Therefore, this layer should have a sufficient thickness and a very low thermal conductivity to be able to reduce the surface temperature of the substrate. Indeed, the order of magnitude of the coatings thickness is generally of several hundred micrometers. Furthermore, they are porous in order to reduce the thermal conductivity. These layers are generally deposited following two processes: by air plasma spraying (APS) or by electron beam physical vapour deposition (EB-PVD). Following the deposition process the coatings present different heterogeneous microstructures [1,2].

This paper is devoted to the study of yttria stabilised zirconia (YSZ) TBC deposited by EB-PVD and particularly to the relationship between deformation mechanisms and mechanical behaviour during a nanoindentation test. There are already a number of papers about TBC by nanoindentation, principally on EB-PVD coatings, generally treating of the effect of aging or the condition of deposition on the measurement of hardness and Young modulus [3-6]. All these studies show the difficulty of measuring the mechanical properties of TBC by nanoindentation due to their heterogeneous structure and their high porosity. The effect of porosity results in a large scatter of the hardness or elastic modulus values which could be reduced by a statistic treatment performed on a large number of experiments. On the other hand, the particular structure of the coatings introduces scale dependence. It is generally observed that, following the depth of indentation, the measured mechanical properties are quite different: at small depth, they are similar to those of the bulk material, while for larger deformation they

are the actual ones of the layer. The shape of the indenter appears also to be predominant [7], since a sharp indenter will probe the coating inside the columns while a flat or a spherical indenter with a high radius a curvature will directly measure the response of the coating.

This paper attempts to establish what is exactly measured by nanoindentation in this type of very heterogeneous coatings. In fact, the analysis of the unloading curves in nanoindentation is based on elastic assumptions [8] valid for continuous solid which is not the case of the TBC. Therefore, attention is paid here to the study of the deformation mechanisms involved during nanoindentation and their correlation with the measured mechanical properties. In particular, we will focus on the scale dependence mainly reported for this type of material.

§ 2. Experimental details:

Yttria stabilised zirconia (YSZ) TBC deposited by EB-PVD, containing 7-8 wt% of yttria have been studied. The upper layer is characterised by a columnar structure and a thickness of 200 µm. The microstructure associated with this process of deposition has been mainly described elsewhere [9]. Figure 1 presents the microstructure of these coatings observed in a plane view by atomic force microscopy (figure 1a) and in cross section by scanning electron microscopy (figure 1b). Particularly, figure 1a shows the arbitrary shape of the columns. The single crystal columns are oriented along the direction of deposition. The porosity of this type of coating has two origins: a) inter-columnar porosity characterised by the space between two columns; b) intra-columnar nano-sized porosity (see figure 1a). The presence of dendrite localised at the column

boundaries contribute also to the increase of porosity (see figure 1b). The average area of the columns on the top coat is 21 μm^2. Before any experiments, the samples were polished because in the as-received conditions they exhibited a surface roughness of several micrometers, which is not compatible with nanoindentation experiments. A final polishing has been performed using colloidal silica.

'[Insert Figure 1 about here]'

Nanoindentation experiments have been performed with a NanoXP (MTS). This nanoindenter is provided with a CSM module (Continuous Stiffness Measurement), which allows a dynamic determination of the Young modulus and hardness during the indentation [10,11]. The values of hardness and Young modulus have been deduced following the Oliver and Pharr method [12]. Furthermore, since this equipment was provided with a high precision positioning table, this nanoindenter allows to obtain topographic images of the sample by scanning the surface with the indenter tip in order to recognize the indentation zone. Two Berkovich indenters, respectively with a tip radius of 40 nm and 700 nm, and a spherical (with a radius of curvature of 25 µm) indenters have been used to probe, in the same range of indentation depth, different contact area of the sample. Diamond indenters having a Young modulus of 1141 GPa and a Poisson coefficient of 0.07 have been used. Atomic force microscopy (AFM) measurements have been carried out to characterise the deformation around the residual imprint. An AFM multimode microscope from Digital Instruments (DI) has been employed. Images were obtained in both contact and tapping mode.

§ 3. Result and discussion:

3.1 Measurement of mechanical properties:

'[Insert Figure 2 about here]'

Nanoindentations have been performed on the top coat of the EB-PVD coatings using the sharp Berkovich indenter. Figure 2 presents the evolution of the Young modulus with indentation depth. Two trends have to be distinguished: firstly, the dispersion for low penetration depth, and, secondly, the decrease of the Young modulus with deformation.

The dispersion can be attributed to the heterogeneous structure of the coatings and particularly to the presence of porosity. In fact, the size of the columns does not allow an accurate optical recognition of the indentation site. It results that a number of nanoindentations are initially performed in or near the porosity localised at the columns boundaries. This type of indentation leads to very low values representative of the very low adhesion between the columns. It is interesting to note that from an indentation depth of about 1000 nm, the mechanical properties of the coating become homogeneous, showing that there is no dependence respected to the initial site of indentation.

Concerning the decrease of the mechanical properties with the deformation, it could be attributed to the difference between the mechanical properties of the bulk YSZ inside the columns and the ones of the coating. In fact the Young modulus of the bulk YSZ is 220 GPa [13] while for the coatings it is reported to be 50-100 GPa [3,4].

'[Insert Figure 3 about here]'

In order to characterise this intra-inter transition, nanoindentation has been performed at the centre of a column. By scanning the surface using the tip of the indenter, the topography of the sample has been captured. A single column has been chosen and indented. The topographic image of the column is presented on figure 3, before and after indentation. The corresponding loading-unloading curve and the evolution of the Young modulus with the indentation depth are also shown on figure 3. The first observation concerns the deformation of the coating. Figure 3b shows that the formation of the residual imprint in the column is accompanied by the sinking-in of the indented column. To characterise more accurately this deformation, AFM observations of the residual imprint has been also performed. The sinking-in behaviour represent about 50 nm of the total residual deformation which is 450 nm, so about 11% of the total residual deformation. As no pop-in effect is observed on the loading-unloading curve (see figure 3c), this sinking-in does not correspond to a sudden behaviour. The indentation has been done inside the column far from the column boundaries, so the modulus measured during the first stages of deformation (180 GPa) is nearly the same as the one of the bulk YSZ. However, this value is still lower than for bulk YSZ because of the presence of intra-columnar porosity. Next, when the indentation reaches a critical value h_1, here 220 nm (figure 3d), the modulus begins to decrease according to the previous observations. The projected contact area Ac_1 corresponding to h_1 and calculated using the O&P method is $1.2*10^6$ nm^2. This contact area has been schematically represented on figure 3b, assuming a perfect shape for the Berkovich indenter. It appears clearly that

this contact area corresponds to an indentation depth were the indenter is still inside the column, even if two of the indenter corners are very close to the column boundary.

Figure 4 shows the surface deformation after four successive indentations performed in the same column respectively at 4.2, 21.6, 53.2 and 137.8 mN. As it is not possible to perform an indentation exactly in the location of the previous one, correct measure of the Young modulus or hardness can not be extracted from these measurements. However, figure 4 demonstrates clearly that the sinking-in of the column occurs only after the third indentation. Taking into account the relatively large amount of elastic recuperation occurring during the unloading in this type of material, it appears that the sinking-in of the columns occurs when the indenter approaches near the column boundaries, that is in the same domain that the decrease of the Young modulus is observed.

'[Insert Figure 4 about here]'

The same phenomenon was observed in several indentations inside single columns. For each test, the Young modulus has shown a plateau and next a decrease of its value until about 89 GPa if the indentation is performed to a sufficient indentation depth. Only the length of the plateau, which appears to be related to the column size, was observed different from one test to another. Although no direct relation can be made between the sinking-in and the evolution of the Young modulus with the deformation, it appears that these two phenomena happen in the same range of indentation depth. As the sinking-in of the column corresponds to the activation an additional inter-columnar mechanism, it could explain the decrease of the Young modulus.

3.2 Influence of the indenter shape:

'[Insert Figure 5 about here]'

In order to clearly correlate the variation of the Young modulus with the microstructure of the coatings, columns exhibiting different size have been indented using the blunt Berkovich indenter (with radius of curvature of 700 nm). Figure 5a shows the evolution of the Young modulus as a function of the penetration depth of the indenter for four indentations performed in four columns with different area with the blunt Berkovich indenter. From this graphic it appears clearly that the size of the columns has a strong influence on the measure of the Young modulus, during the first stages of deformation. In fact, it is observed that more the columns is smaller more the Young modulus decrease rapidly. This is completely coherent with the explanation proposed before which state that the sinking-in of the columns occurs when the indenter is still inside the column and coincides with the decrease of the Young modulus. Furthermore, a special attention can be paid to figure 5b where the evolution of the Young modulus corresponding to two indentations performed respectively with the sharp and the blunt Berkovich indenter in two columns of a similar area (34 and 33 μm^2). It is observed that the Young modulus decrease more rapidly in the case of the blunt Berkovich because, as the tip radius is higher for the blunt Berkovich indenter, its lateral extension at the surface of the columns during the indentation is higher than the sharp one for the same range of penetration depth. This also shows that it is more difficult to probe the mechanical properties of the YSZ inside the columns with the blunt than with the sharp indenter.

To explore the effect of the indenter shape a spherical indenter having a radius of curvature of 25 µm has also been used to characterise these coatings. This type of indenter, in comparison with the Berkovich indenter, allows to have very different contact area for equivalent penetration depth (See figure 6a). Consequently it allows extending the plastic zone to a higher number of columns (as it is observed on the optical micrograph on figure 6b). The curve presented on figure 6b shows the evolution of the Young modulus measured with the spherical indenter as a function of indenter penetration depth. One can observe that the values of the Young modulus reach a constant value of 83 GPa for penetration depth higher than 300 nm. This modulus is very similar to the value of 89 GPa obtained with the Berkovich indenter. Furthermore, this value is reached for penetration depth lower than the one involved with the Berkovich indenter (1000 nm) as the contact area is higher for the spherical than for the Berkovich indenter for the same penetration depth of indentation (See figure 6a). An interesting feature is also observed before indentation depths of 300 nm. It appears that for all the indentations very low Young modulus are measured during the first stages of deformation, which indicates that the use of the spherical indenter does not allow probing the bulk YSZ inside the columns.

'[Insert Figure 6 about here]'

The experiments performed with the sharp Berkovich indenter have shown that, respected to the average size of the columns and taking into account that the stressed area is several times the contact area, the mechanical properties of the bulk material inside the columns can be correctly determined for penetration depth between 0 and 250

nm. For higher penetration depth the measured mechanical properties appear to depend of inter-columnar deformation mechanisms (sinking-in). In the case of the spherical indenter, respecting to the contact area involved during the indentation (see figure 6a), this depth range becomes between 0 and 11 nm. In this depth range, taking into account that the CSM amplitude is 2 nm and the roughness of the surface is 4 nm inside the column, it is difficult to determine a proper value of the Young modulus. So, it can be assumed that in the case of spherical indentation, since the first stages of deformation (at least for penetration depth higher than 11 nm), the stresses at the columns boundaries are sufficient to cause the sinking-in of the indented column. The indenter probes directly the adhesion between the columns, explaining the very low values of Young modulus encountered between 0 and 300 nm. This is supported by the fact that the loading-unloading curves have not shown pure elastic regime as it could be expected in the case of spherical indentations in single crystal ceramics [14].

'[Insert Figure 7 about here]'

Figure 7 shows the AFM images obtained around an indentation performed at a maximum load of 400 mN (for a maximum penetration depth of 900 nm), leading to a residual penetration of 300 nm. One can observe that the surrounding deformation around the residual imprint is mainly characterised by the sinking-in of all the adjacent columns. The sinking-in of the columns represents about 50% of the total residual deformation (150 nm of sinking-in for a residual deformation of 300 nm). The sinking-in of surrounding columns has been also observed around sharp indentation for indentation depth higher than 1500 nm. This regime of deformation corresponds to the extension of the initial imprint where the plastic deformation is accommodated by the

sinking-in of the columns. It is also independent of the indenter shape and may correspond to the extension of a pyramidal as well as that the one of a spherical imprint and this is the reason for the Young modulus encountered for Berkovich and spherical indentation were nearly the same.

§ 4. Conclusion:

YSZ EB-PVD thermal barriers coatings have been investigated using nanoindentation and AFM. In particular, the attention has been focused on the connection between Young modulus and the columnar microstructure of the coatings. It leads to the following conclusions:

1. The use of indenters with different shapes has shown that the size of the probed contact area, respected to the size of the column, is the parameter characteristic of the scale dependence of the Young modulus.

2. It has been shown that the deformation of these coatings is accompanied by the sinking-in of the columns involved under the indenter.

3. During the first stage of deformation, the very high localised stresses involved during a sharp indentation minimize the effect of this sinking-in and conduct to the measure of mechanical properties close to the ones of the bulk YSZ. On the other hand, the enlargement of the stressed zone during a spherical indentation (with a large radius of curvature), particularly at the columns boundaries, promotes the sinking-in of the indented column since the first stage of deformations.

4. Whatever the indenter shape, the deformation stage corresponding to the extension of the initial imprint can be understood by the sinking-in of the adjacent columns,

accommodating the irreversible deformation. The Young modulus measured during this stage of deformation is nearly the same with the two indenters and appear independent of the location of the initial contact.

Acknowledgements:

Work supported by the European Community's Human Potential Programme under contract HPRN-CT-2002-00203, [SICMAC]. Y.G. acknowledges the financial support provided through the European Community's Human Potential Programme under contract HPRN-CT-2002-00203, [SICMAC]. The authors acknowledge Marion Bartsch for providing the EB-PVD specimens.

References:

[1] J.A. Thompson, and T.W. Clyne, *Acta Materialia*, 49, 2001, 1565.

[2] A.G. Evans, D.R. Mumm, J.W. Hutchinson, G.H. Meier, F.S. Pettit, *Progress in material science*, 46, 2001, 505.

[3] E. Lugscheider, K. Bozbin, S. Barwulf, A. Etzkorn, *Surface and Coatings Technology*, 138, 2001, 9.

[4] R.G. Wellman, H. Tourmente, S. Impey, and J.R. Nicholls, *Surface and Coatings Technology*, 188-189, 2004, 79.

[5] S. Guo, Y. Kagawa, *Surface and Coatings Technology*, 182, 2004, 92.

[6] B.K. Jang, H. Matsubara, *Material Letter*, 2005.

[7] J. Malzbender and R.W. Steinbrech, *Journal of material research*, 8, 2003, 1975.

[8] I.N. Sneddon, *International Journal of Engineering Science*, 3, 1965, 47.

[9] U. Schulz, M. Schmucker, *Material science and Engineering A*, 276, 2000, 1.

[10] X. Li, and B. Bushan, *Materials Characterisation*, 48, 2002, 11.

[11] W.C. Oliver, G.M. Pharr, *Journal of Material Research*, 1, 2004, 3.

[12] W.C. Oliver, G.M. Pharr, *Journal of Material Research*, 7, 1992, 1564.

[13] A. Selcuk, and A. Atkinson, *Journal of the American ceramic society*, 17, 1997, 1523.

[14] Y. Gaillard, C. Tromas, J. Woirgard, *Acta Materialia*, 54, 2006, 1409.

Figures :

Figure 1: Microstructure of the EB-PVD coatings. (a) AFM contact mode images of the plane view (b) Cross-section obtained by focused ion beam and observed by SEM. The magnifications allow to enhance the dendrites at the columns boundaries and the nano-sized porosity inside the columns.

Figure 2: Evolution of the Young modulus with the indentation depth measured with the sharp Berkovich indenter for 15 indentations.

Figure 3: Topography of the sample before (a) and after (b) an indentation performed at 85mN. The corresponding loading-unloading curve is presented in (c) and the evolution of the Young modulus during the indentation in (d).

Figure 4: Series of topographic images obtained by scanning the surface with the indenter tip after several indentations performed respectively at 4.2, 21.6, 53.2 and 137.8 mN in the same column. It is interesting to note that the sinking-in of the indented column occurs only after the third indentation.

Figure 5: (a) Evolution of the Young modulus as a function of the penetration depth of the indenter for four indentations performed in four columns exhibiting respectively

area of 16, 33, 55 and 67 μm^2. (b) Comparison between the evolutions of the Young modulus of two indentations performed respectively with the sharp and the blunt Berkovich indenters in two columns having a similar area, 34 and 33 μm^2.

Figure 6: (a) Comparison of the projected contact area involved during indentation with the sharp Berkovich and the spherical indenters (b) Evolution of the Young modulus with the indentation depth measured with the spherical indenter for 15 indentations. An optical micrograph of a spherical indentation performed until a penetration depth of 5000 nm is also shown.

Figure 7: AFM images of a spherical indentation performed at 400 mN and leading to a residual penetration depth of 300 nm.

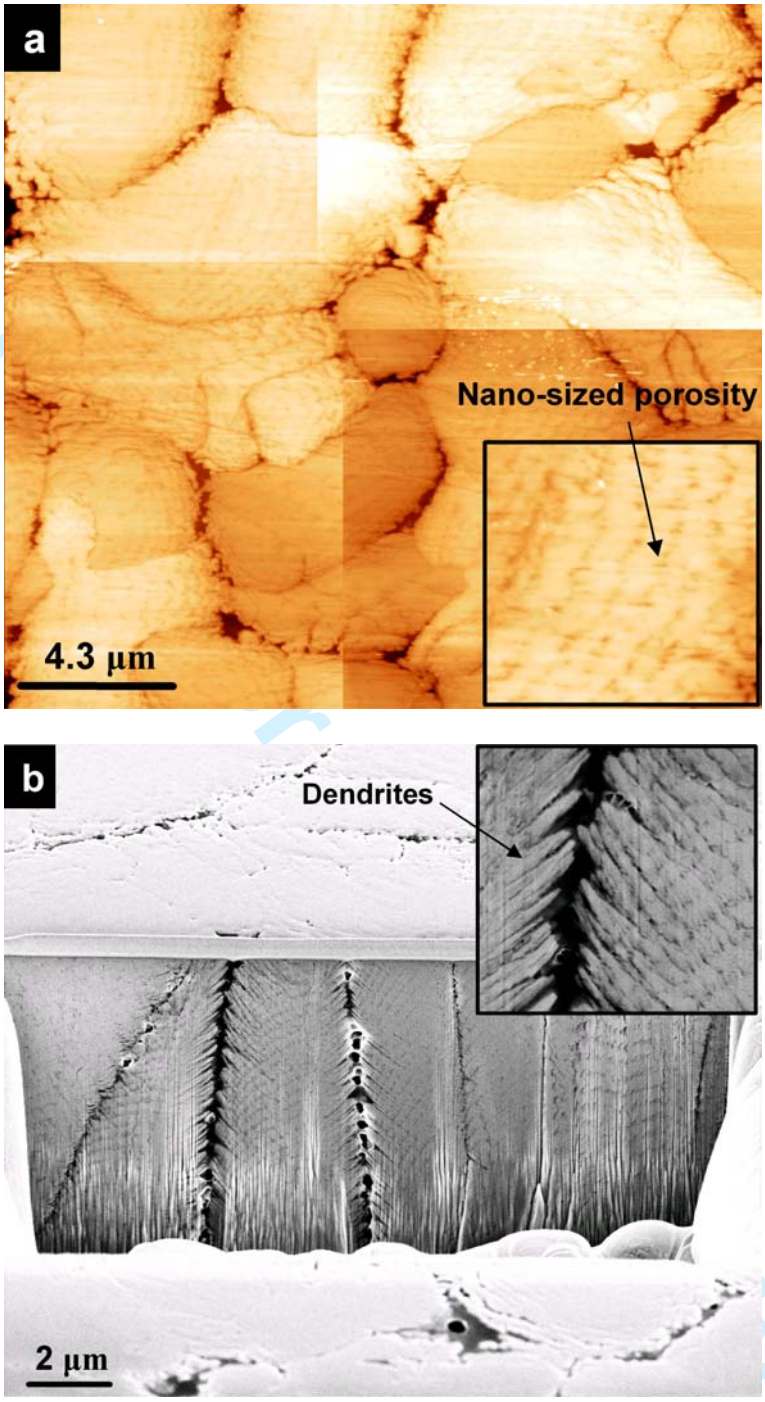

Figure 1

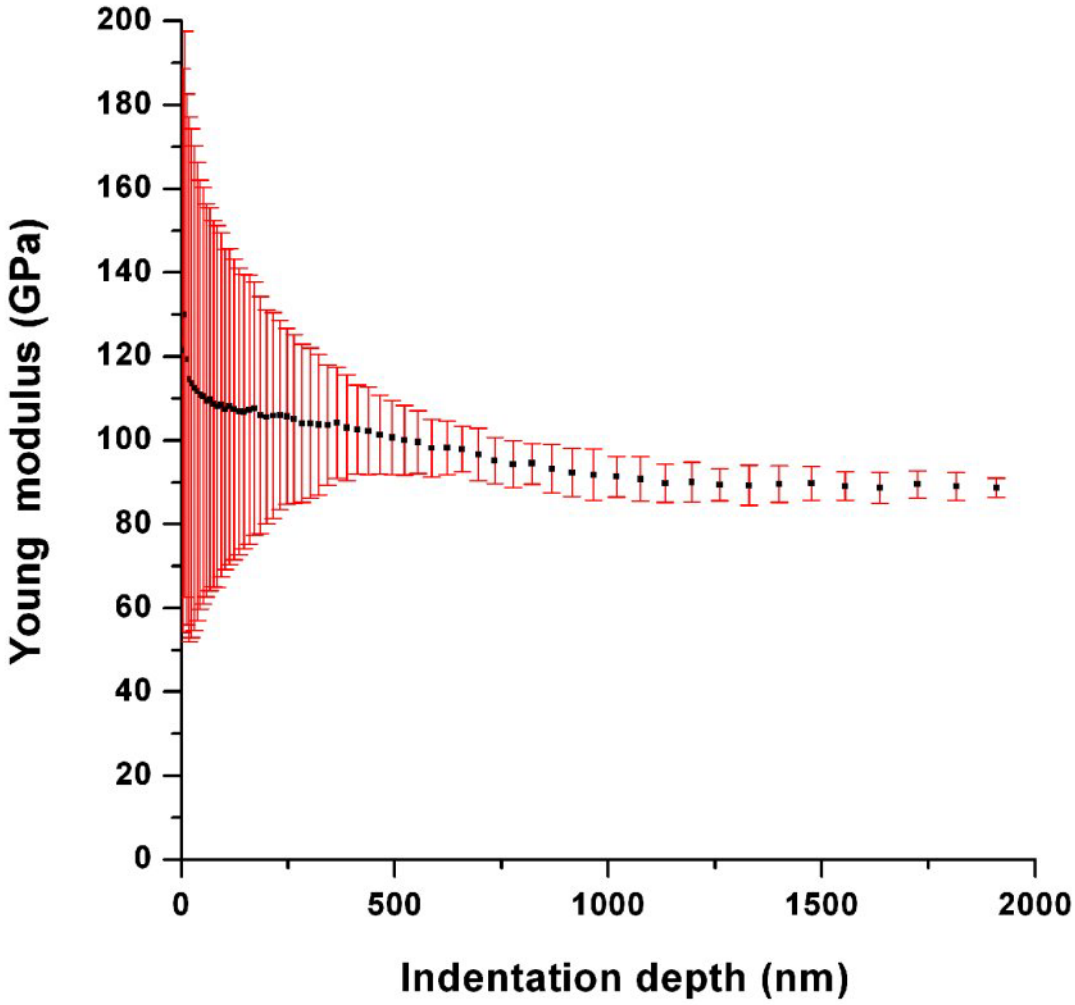

Figure2

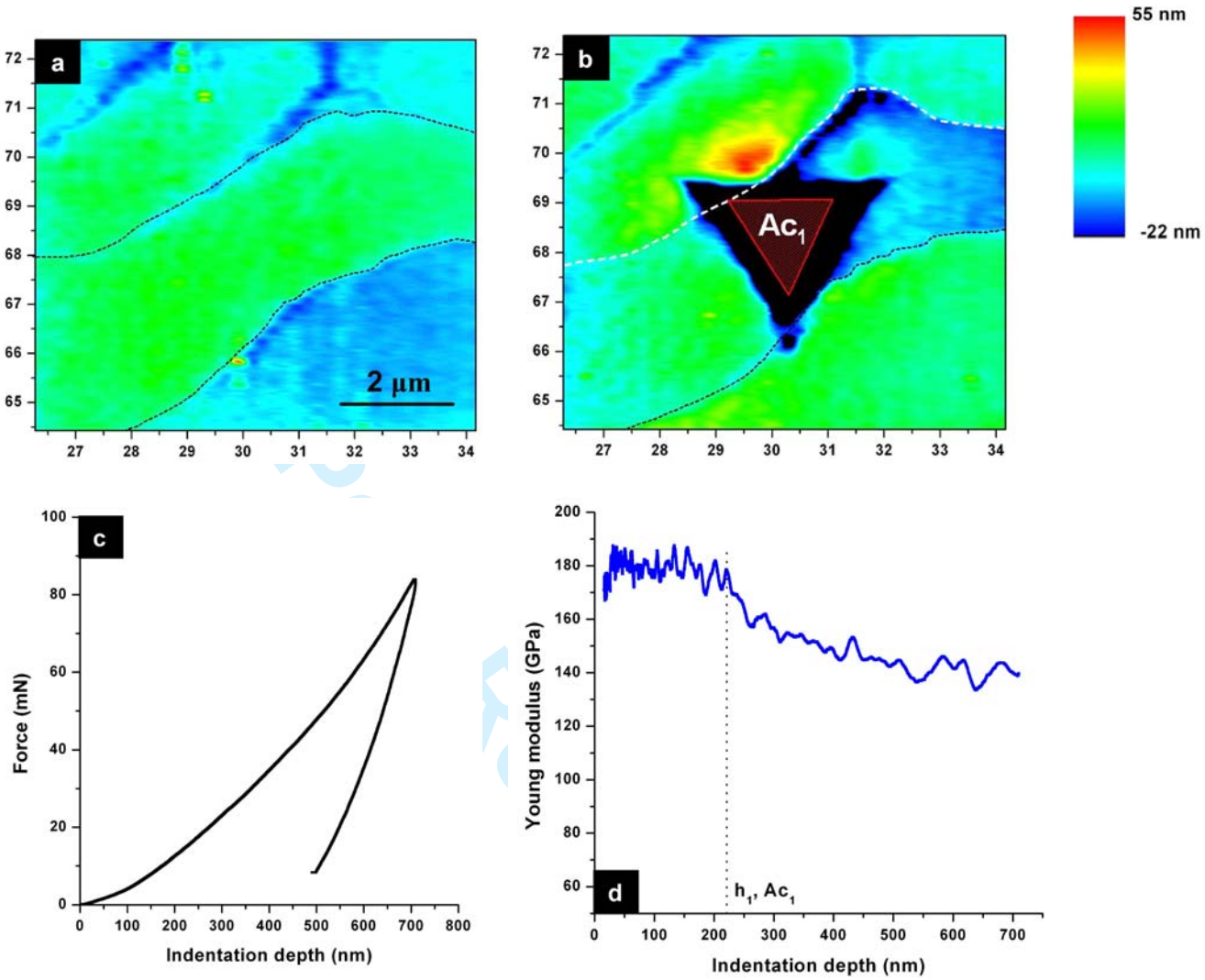
a
b
c
d
55 nm
-22 nm
2 µm
Ac1
Force (mN)
Indentation depth (nm)
Young modulus (GPa)
h1, Ac1
Indentation depth (nm)

Figure3

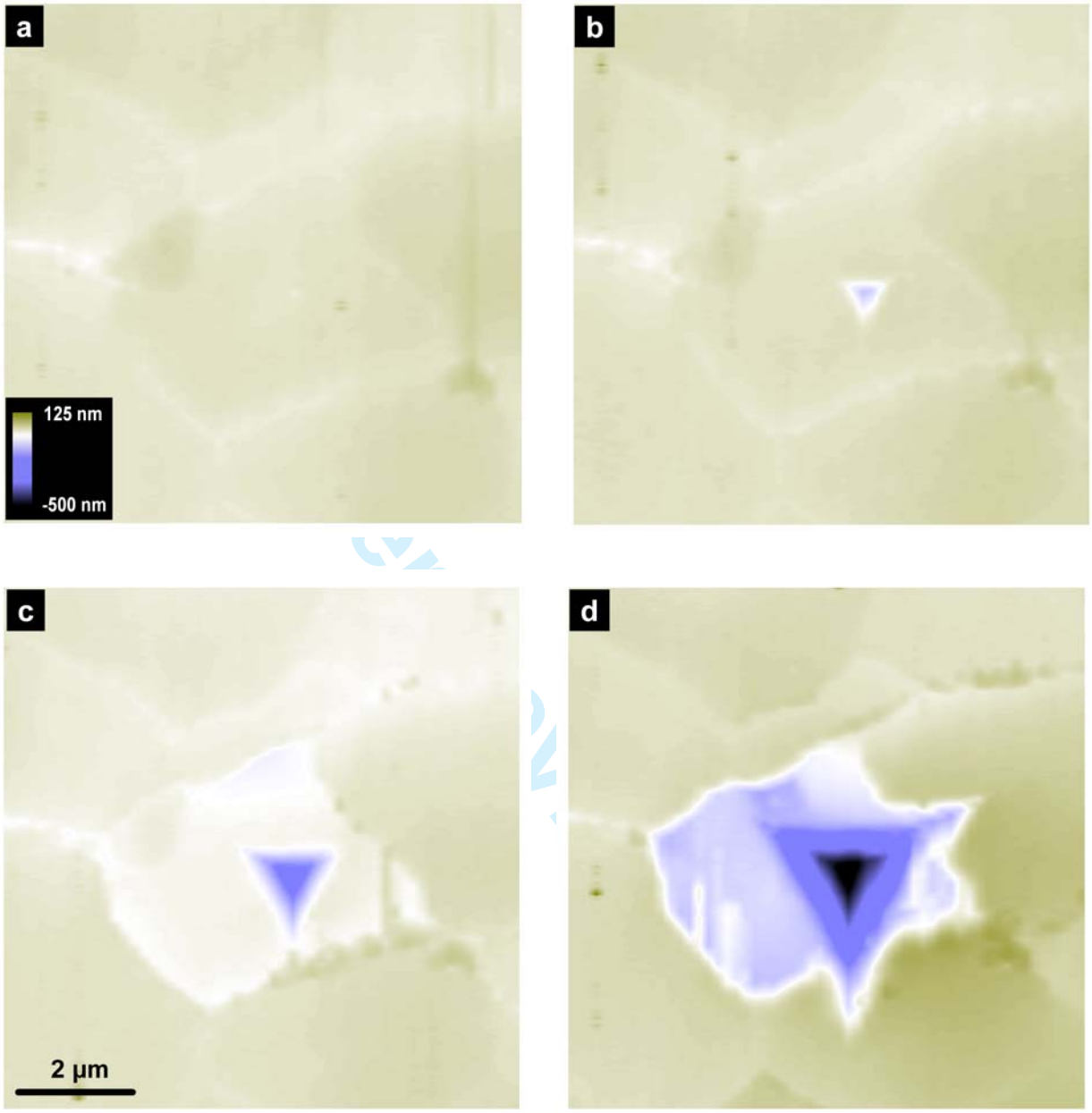

Figure 4

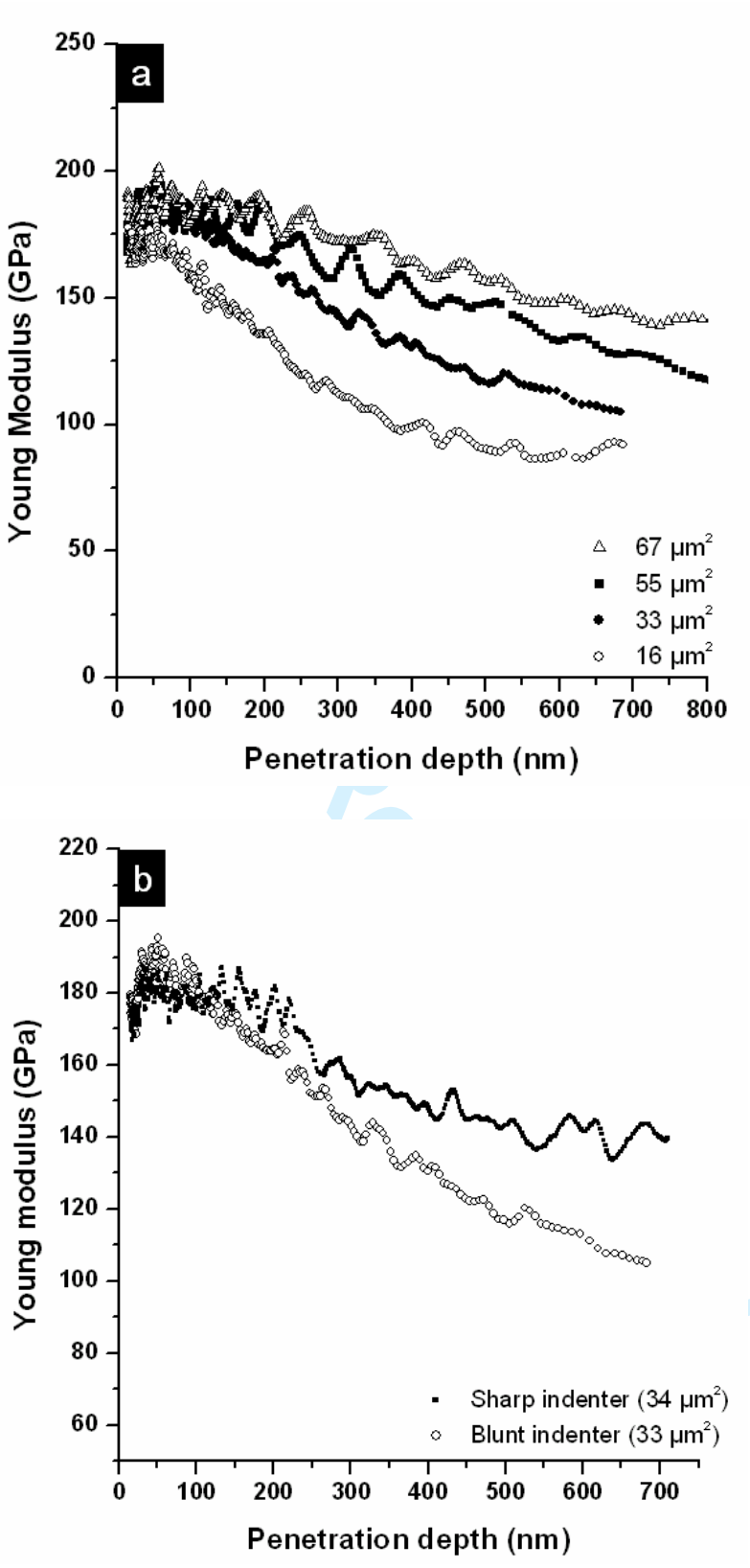
a
Young Modulus (GPa)
Penetration depth (nm)
67 μm²
55 μm²
33 μm²
16 μm²
b
Young modulus (GPa)
Penetration depth (nm)
Sharp indenter (34 μm²)
Blunt indenter (33 μm²)

Figure 5

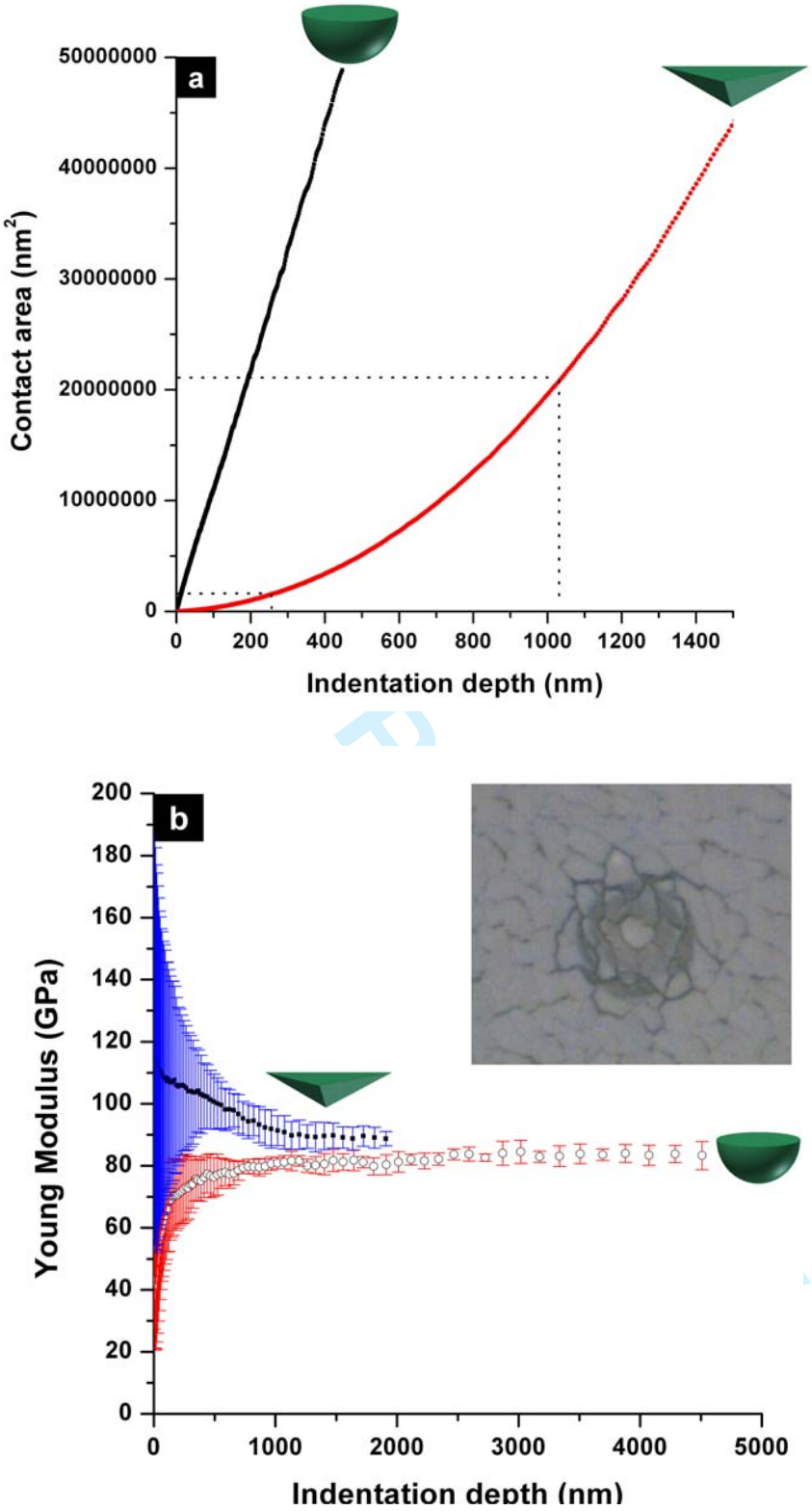
a
Contact area (nm^2)
50000000
40000000
30000000
20000000
10000000
0
0
200
400
600
800
1000
1200
1400
Indentation depth (nm)
b
Young Modulus (GPa)
200
180
160
140
120
100
80
60
40
20
0
0
1000
2000
3000
4000
5000
Indentation depth (nm)

Figure 6

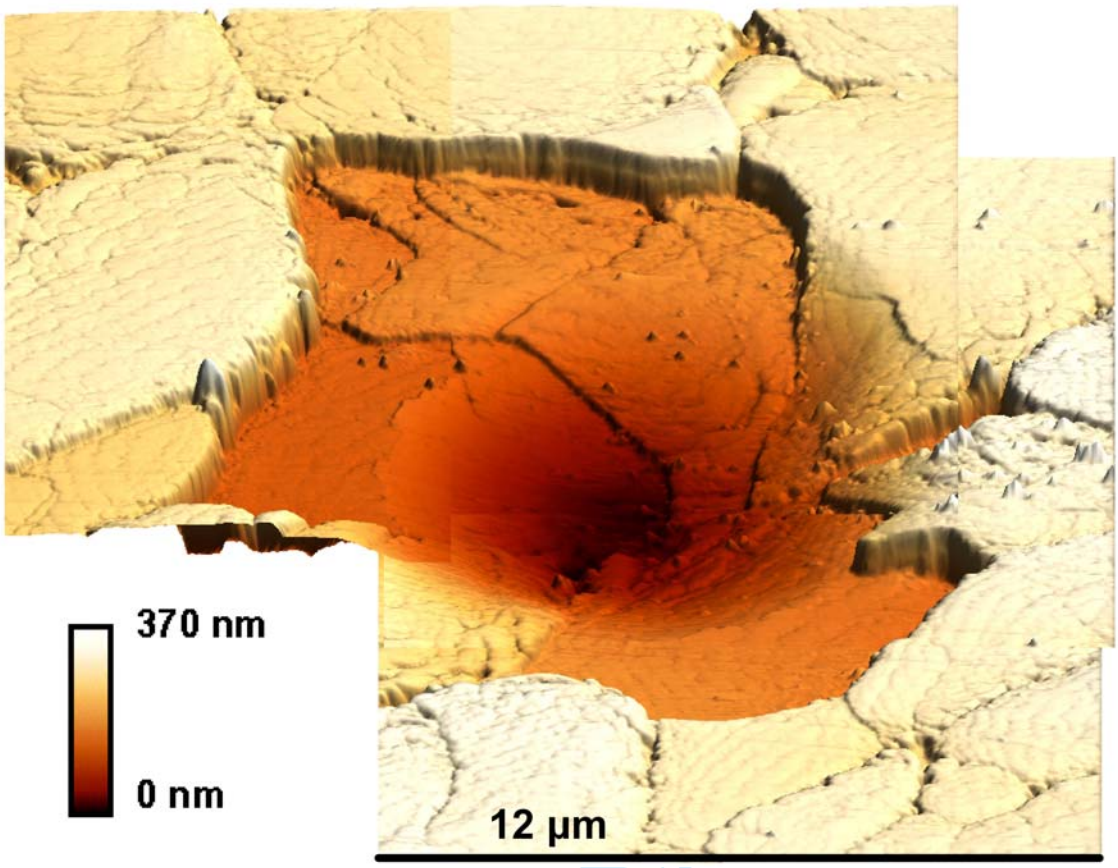

Figure 7

Scale dependence of the Young modulus measured by nanoindentation in columnar YSZ EB-PVD thermal barriers coatings

Y. GAILLARD, E. JIMENEZ-PIQUE and M. ANGLADA

Department of Materials Science and Metallurgy (CMEM), Universitat Politécnica de Catalunya, Avda. Diagonal 647 (ETSEIB), 08028 Barcelona, Spain.

Abstract :

Electron beam physical vapour deposited yttria stabilised zirconia (YSZ) thermal barrier coatings have been investigated by nanoindentation. It is shown that the mechanical properties, and particularly the Young modulus, of these coatings are closely related to their columnar microstructure. The transition from intra-columnar to inter-columnar deformation is characterised by a difference between the mechanical properties of the bulk YSZ and the ones of the coatings. The use of different indenter shape showed that the contact area was the parameter characteristic of this scale dependence. The deformation mechanisms studied by AFM have shown a good correlation with the evolution of the mechanical properties during the deformation.

Keywords : Thermal barrier coatings, nanoindentation, EB-PVD, AFM.

§ 1.Introduction :

Thermal barriers coatings (TBC) are widely used in the aircraft industry as protective coatings for gas engines turbine components. These tri-layered materials are composed

of an intermetallic bond coat (BC) deposited on a substrate, generally a super-alloy, and a ceramic top coat deposited on the bond coat. A thermally growth oxide (TGO) localised between the BC and the top coat is also formed during the deposition. The bond coat is an oxidation protection for the alloy while the top coat acts as the thermal insulator. Therefore, this layer should have a sufficient thickness and a very low thermal conductivity to be able to reduce the surface temperature of the substrate. Indeed, the order of magnitude of the coatings thickness is generally of several hundred micrometers. Furthermore, they are porous in order to reduce the thermal conductivity. These layers are generally deposited following two processes: by air plasma spraying (APS) or by electron beam physical vapour deposition (EB-PVD). Following the deposition process the coatings present different heterogeneous microstructures [1,2].

This paper is devoted to the study of yttria stabilised zirconia (YSZ) TBC deposited by EB-PVD and particularly to the relationship between deformation mechanisms and mechanical behaviour during a nanoindentation test. There are already a number of papers about TBC by nanoindentation, principally on EB-PVD coatings, generally treating of the effect of aging or the condition of deposition on the measurement of hardness and Young modulus [3-6]. All these studies show the difficulty of measuring the mechanical properties of TBC by nanoindentation due to their heterogeneous structure and their high porosity. The effect of porosity results in a large scatter of the hardness or elastic modulus values which could be reduced by a statistic treatment performed on a large number of experiments. On the other hand, the particular structure of the coatings introduces scale dependence. It is generally observed that, following the depth of indentation, the measured mechanical properties are quite different: at small depth, they are similar to those of the bulk material, while for larger deformation they

are the actual ones of the layer. The shape of the indenter appears also to be predominant [7], since a sharp indenter will probe the coating inside the columns while a flat or a spherical indenter with a high radius a curvature will directly measure the response of the coating.

This paper attempts to establish what is exactly measured by nanoindentation in this type of very heterogeneous coatings. In fact, the analysis of the unloading curves in nanoindentation is based on elastic assumptions [8] valid for continuous solid which is not the case of the TBC. Therefore, attention is paid here to the study of the deformation mechanisms involved during nanoindentation and their correlation with the measured mechanical properties. In particular, we will focus on the scale dependence mainly reported for this type of material.

§ 2. Experimental details:

Yttria stabilised zirconia (YSZ) TBC deposited by EB-PVD, containing 7-8 wt% of yttria have been studied. The upper layer is characterised by a columnar structure and a thickness of 200 µm. The microstructure associated with this process of deposition has been mainly described elsewhere [9]. Figure 1 presents the microstructure of these coatings observed in a plane view by atomic force microscopy (figure 1a) and in cross section by scanning electron microscopy (figure 1b). Particularly, figure 1a shows the arbitrary shape of the columns. The single crystal columns are oriented along the direction of deposition. The porosity of this type of coating has two origins: a) inter-columnar porosity characterised by the space between two columns; b) intra-columnar nano-sized porosity (see figure 1a). The presence of dendrite localised at the column

boundaries contribute also to the increase of porosity (see figure 1b). The average area of the columns on the top coat is 21 μm^2. Before any experiments, the samples were polished because in the as-received conditions they exhibited a surface roughness of several micrometers, which is not compatible with nanoindentation experiments. A final polishing has been performed using colloidal silica.

'[Insert Figure 1 about here]'

Nanoindentation experiments have been performed with a NanoXP (MTS). This nanoindenter is provided with a CSM module (Continuous Stiffness Measurement), which allows a dynamic determination of the Young modulus and hardness during the indentation [10,11]. The values of hardness and Young modulus have been deduced following the Oliver and Pharr method [12]. Furthermore, since this equipment was provided with a high precision positioning table, this nanoindenter allows to obtain topographic images of the sample by scanning the surface with the indenter tip in order to recognize the indentation zone. Two Berkovich indenters, respectively with a tip radius of 40 nm and 700 nm, and a spherical (with a radius of curvature of 25 µm) indenters have been used to probe, in the same range of indentation depth, different contact area of the sample. Diamond indenters having a Young modulus of 1141 GPa and a Poisson coefficient of 0.07 have been used. Atomic force microscopy (AFM) measurements have been carried out to characterise the deformation around the residual imprint. An AFM multimode microscope from Digital Instruments (DI) has been employed. Images were obtained in both contact and tapping mode.

§ 3. Result and discussion:

3.1 Measurement of mechanical properties:

'[Insert Figure 2 about here]'

Nanoindentations have been performed on the top coat of the EB-PVD coatings using the sharp Berkovich indenter. Figure 2 presents the evolution of the Young modulus with indentation depth. Two trends have to be distinguished: firstly, the dispersion for low penetration depth, and, secondly, the decrease of the Young modulus with deformation.

The dispersion can be attributed to the heterogeneous structure of the coatings and particularly to the presence of porosity. In fact, the size of the columns does not allow an accurate optical recognition of the indentation site. It results that a number of nanoindentations are initially performed in or near the porosity localised at the columns boundaries. This type of indentation leads to very low values representative of the very low adhesion between the columns. It is interesting to note that from an indentation depth of about 1000 nm, the mechanical properties of the coating become homogeneous, showing that there is no dependence respected to the initial site of indentation.

Concerning the decrease of the mechanical properties with the deformation, it could be attributed to the difference between the mechanical properties of the bulk YSZ inside the columns and the ones of the coating. In fact the Young modulus of the bulk YSZ is 220 GPa [13] while for the coatings it is reported to be 50-100 GPa [3,4].

'[Insert Figure 3 about here]'

In order to characterise this intra-inter transition, nanoindentation has been performed at the centre of a column. By scanning the surface using the tip of the indenter, the topography of the sample has been captured. A single column has been chosen and indented. The topographic image of the column is presented on figure 3, before and after indentation. The corresponding loading-unloading curve and the evolution of the Young modulus with the indentation depth are also shown on figure 3. The first observation concerns the deformation of the coating. Figure 3b shows that the formation of the residual imprint in the column is accompanied by the sinking-in of the indented column. To characterise more accurately this deformation, AFM observations of the residual imprint has been also performed. The sinking-in behaviour represent about 50 nm of the total residual deformation which is 450 nm, so about 11% of the total residual deformation. As no pop-in effect is observed on the loading-unloading curve (see figure 3c), this sinking-in does not correspond to a sudden behaviour. The indentation has been done inside the column far from the column boundaries, so the modulus measured during the first stages of deformation (180 GPa) is nearly the same as the one of the bulk YSZ. However, this value is still lower than for bulk YSZ because of the presence of intra-columnar porosity. Next, when the indentation reaches a critical value h_1, here 220 nm (figure 3d), the modulus begins to decrease according to the previous observations. The projected contact area Ac_1 corresponding to h_1 and calculated using the O&P method is $1.2*10^6$ nm^2. This contact area has been schematically represented on figure 3b, assuming a perfect shape for the Berkovich indenter. It appears clearly that

this contact area corresponds to an indentation depth were the indenter is still inside the column, even if two of the indenter corners are very close to the column boundary.

Figure 4 shows the surface deformation after four successive indentations performed in the same column respectively at 4.2, 21.6, 53.2 and 137.8 mN. As it is not possible to perform an indentation exactly in the location of the previous one, correct measure of the Young modulus or hardness can not be extracted from these measurements. However, figure 4 demonstrates clearly that the sinking-in of the column occurs only after the third indentation. Taking into account the relatively large amount of elastic recuperation occurring during the unloading in this type of material, it appears that the sinking-in of the columns occurs when the indenter approaches near the column boundaries, that is in the same domain that the decrease of the Young modulus is observed.

'[Insert Figure 4 about here]'

The same phenomenon was observed in several indentations inside single columns. For each test, the Young modulus has shown a plateau and next a decrease of its value until about 89 GPa if the indentation is performed to a sufficient indentation depth. Only the length of the plateau, which appears to be related to the column size, was observed different from one test to another. Although no direct relation can be made between the sinking-in and the evolution of the Young modulus with the deformation, it appears that these two phenomena happen in the same range of indentation depth. As the sinking-in of the column corresponds to the activation an additional inter-columnar mechanism, it could explain the decrease of the Young modulus.

3.2 Influence of the indenter shape:

'[Insert Figure 5 about here]'

In order to clearly correlate the variation of the Young modulus with the microstructure of the coatings, columns exhibiting different size have been indented using the blunt Berkovich indenter (with radius of curvature of 700 nm). Figure 5a shows the evolution of the Young modulus as a function of the penetration depth of the indenter for four indentations performed in four columns with different area with the blunt Berkovich indenter. From this graphic it appears clearly that the size of the columns has a strong influence on the measure of the Young modulus, during the first stages of deformation. In fact, it is observed that more the columns is smaller more the Young modulus decrease rapidly. This is completely coherent with the explanation proposed before which state that the sinking-in of the columns occurs when the indenter is still inside the column and coincides with the decrease of the Young modulus. Furthermore, a special attention can be paid to figure 5b where the evolution of the Young modulus corresponding to two indentations performed respectively with the sharp and the blunt Berkovich indenter in two columns of a similar area (34 and 33 μm^2). It is observed that the Young modulus decrease more rapidly in the case of the blunt Berkovich because, as the tip radius is higher for the blunt Berkovich indenter, its lateral extension at the surface of the columns during the indentation is higher than the sharp one for the same range of penetration depth. This also shows that it is more difficult to probe the mechanical properties of the YSZ inside the columns with the blunt than with the sharp indenter.

To explore the effect of the indenter shape a spherical indenter having a radius of curvature of 25 µm has also been used to characterise these coatings. This type of indenter, in comparison with the Berkovich indenter, allows to have very different contact area for equivalent penetration depth (See figure 6a). Consequently it allows extending the plastic zone to a higher number of columns (as it is observed on the optical micrograph on figure 6b). The curve presented on figure 6b shows the evolution of the Young modulus measured with the spherical indenter as a function of indenter penetration depth. One can observe that the values of the Young modulus reach a constant value of 83 GPa for penetration depth higher than 300 nm. This modulus is very similar to the value of 89 GPa obtained with the Berkovich indenter. Furthermore, this value is reached for penetration depth lower than the one involved with the Berkovich indenter (1000 nm) as the contact area is higher for the spherical than for the Berkovich indenter for the same penetration depth of indentation (See figure 6a). An interesting feature is also observed before indentation depths of 300 nm. It appears that for all the indentations very low Young modulus are measured during the first stages of deformation, which indicates that the use of the spherical indenter does not allow probing the bulk YSZ inside the columns.

'[Insert Figure 6 about here]'

The experiments performed with the sharp Berkovich indenter have shown that, respected to the average size of the columns and taking into account that the stressed area is several times the contact area, the mechanical properties of the bulk material inside the columns can be correctly determined for penetration depth between 0 and 250

nm. For higher penetration depth the measured mechanical properties appear to depend of inter-columnar deformation mechanisms (sinking-in). In the case of the spherical indenter, respecting to the contact area involved during the indentation (see figure 6a), this depth range becomes between 0 and 11 nm. In this depth range, taking into account that the CSM amplitude is 2 nm and the roughness of the surface is 4 nm inside the column, it is difficult to determine a proper value of the Young modulus. So, it can be assumed that in the case of spherical indentation, since the first stages of deformation (at least for penetration depth higher than 11 nm), the stresses at the columns boundaries are sufficient to cause the sinking-in of the indented column. The indenter probes directly the adhesion between the columns, explaining the very low values of Young modulus encountered between 0 and 300 nm. This is supported by the fact that the loading-unloading curves have not shown pure elastic regime as it could be expected in the case of spherical indentations in single crystal ceramics [14].

'[Insert Figure 7 about here]'

Figure 7 shows the AFM images obtained around an indentation performed at a maximum load of 400 mN (for a maximum penetration depth of 900 nm), leading to a residual penetration of 300 nm. One can observe that the surrounding deformation around the residual imprint is mainly characterised by the sinking-in of all the adjacent columns. The sinking-in of the columns represents about 50% of the total residual deformation (150 nm of sinking-in for a residual deformation of 300 nm). The sinking-in of surrounding columns has been also observed around sharp indentation for indentation depth higher than 1500 nm. This regime of deformation corresponds to the extension of the initial imprint where the plastic deformation is accommodated by the

sinking-in of the columns. It is also independent of the indenter shape and may correspond to the extension of a pyramidal as well as that the one of a spherical imprint and this is the reason for the Young modulus encountered for Berkovich and spherical indentation were nearly the same.

§ 4. Conclusion:

YSZ EB-PVD thermal barriers coatings have been investigated using nanoindentation and AFM. In particular, the attention has been focused on the connection between Young modulus and the columnar microstructure of the coatings. It leads to the following conclusions:

1. The use of indenters with different shapes has shown that the size of the probed contact area, respected to the size of the column, is the parameter characteristic of the scale dependence of the Young modulus.

2. It has been shown that the deformation of these coatings is accompanied by the sinking-in of the columns involved under the indenter.

3. During the first stage of deformation, the very high localised stresses involved during a sharp indentation minimize the effect of this sinking-in and conduct to the measure of mechanical properties close to the ones of the bulk YSZ. On the other hand, the enlargement of the stressed zone during a spherical indentation (with a large radius of curvature), particularly at the columns boundaries, promotes the sinking-in of the indented column since the first stage of deformations.

4. Whatever the indenter shape, the deformation stage corresponding to the extension of the initial imprint can be understood by the sinking-in of the adjacent columns,

accommodating the irreversible deformation. The Young modulus measured during this stage of deformation is nearly the same with the two indenters and appear independent of the location of the initial contact.

Acknowledgements:

Work supported by the European Community's Human Potential Programme under contract HPRN-CT-2002-00203, [SICMAC]. Y.G. acknowledges the financial support provided through the European Community's Human Potential Programme under contract HPRN-CT-2002-00203, [SICMAC]. The authors acknowledge Marion Bartsch for providing the EB-PVD specimens.

References:

[1] J.A. Thompson, and T.W. Clyne, *Acta Materialia*, 49, 2001, 1565.

[2] A.G. Evans, D.R. Mumm, J.W. Hutchinson, G.H. Meier, F.S. Pettit, *Progress in material science*, 46, 2001, 505.

[3] E. Lugscheider, K. Bozbin, S. Barwulf, A. Etzkorn, *Surface and Coatings Technology*, 138, 2001, 9.

[4] R.G. Wellman, H. Tourmente, S. Impey, and J.R. Nicholls, *Surface and Coatings Technology*, 188-189, 2004, 79.

[5] S. Guo, Y. Kagawa, *Surface and Coatings Technology*, 182, 2004, 92.

[6] B.K. Jang, H. Matsubara, *Material Letter*, 2005.

[7] J. Malzbender and R.W. Steinbrech, *Journal of material research*, 8, 2003, 1975.

[8] I.N. Sneddon, *International Journal of Engineering Science*, 3, 1965, 47.

[9] U. Schulz, M. Schmucker, *Material science and Engineering A*, 276, 2000, 1.

[10] X. Li, and B. Bushan, *Materials Characterisation*, 48, 2002, 11.

[11] W.C. Oliver, G.M. Pharr, *Journal of Material Research*, 1, 2004, 3.

[12] W.C. Oliver, G.M. Pharr, *Journal of Material Research*, 7, 1992, 1564.

[13] A. Selcuk, and A. Atkinson, *Journal of the American ceramic society*, 17, 1997, 1523.

[14] Y. Gaillard, C. Tromas, J. Woirgard, *Acta Materialia*, 54, 2006, 1409.

Figures :

Figure 1: Microstructure of the EB-PVD coatings. (a) AFM contact mode images of the plane view (b) Cross-section obtained by focused ion beam and observed by SEM. The magnifications allow to enhance the dendrites at the columns boundaries and the nano-sized porosity inside the columns.

Figure 2: Evolution of the Young modulus with the indentation depth measured with the sharp Berkovich indenter for 15 indentations.

Figure 3: Topography of the sample before (a) and after (b) an indentation performed at 85mN. The corresponding loading-unloading curve is presented in (c) and the evolution of the Young modulus during the indentation in (d).

Figure 4: Series of topographic images obtained by scanning the surface with the indenter tip after several indentations performed respectively at 4.2, 21.6, 53.2 and 137.8 mN in the same column. It is interesting to note that the sinking-in of the indented column occurs only after the third indentation.

Figure 5: (a) Evolution of the Young modulus as a function of the penetration depth of the indenter for four indentations performed in four columns exhibiting respectively

area of 16, 33, 55 and 67 μm^2. (b) Comparison between the evolutions of the Young modulus of two indentations performed respectively with the sharp and the blunt Berkovich indenters in two columns having a similar area, 34 and 33 μm^2.

Figure 6: (a) Comparison of the projected contact area involved during indentation with the sharp Berkovich and the spherical indenters (b) Evolution of the Young modulus with the indentation depth measured with the spherical indenter for 15 indentations. An optical micrograph of a spherical indentation performed until a penetration depth of 5000 nm is also shown.

Figure 7: AFM images of a spherical indentation performed at 400 mN and leading to a residual penetration depth of 300 nm.

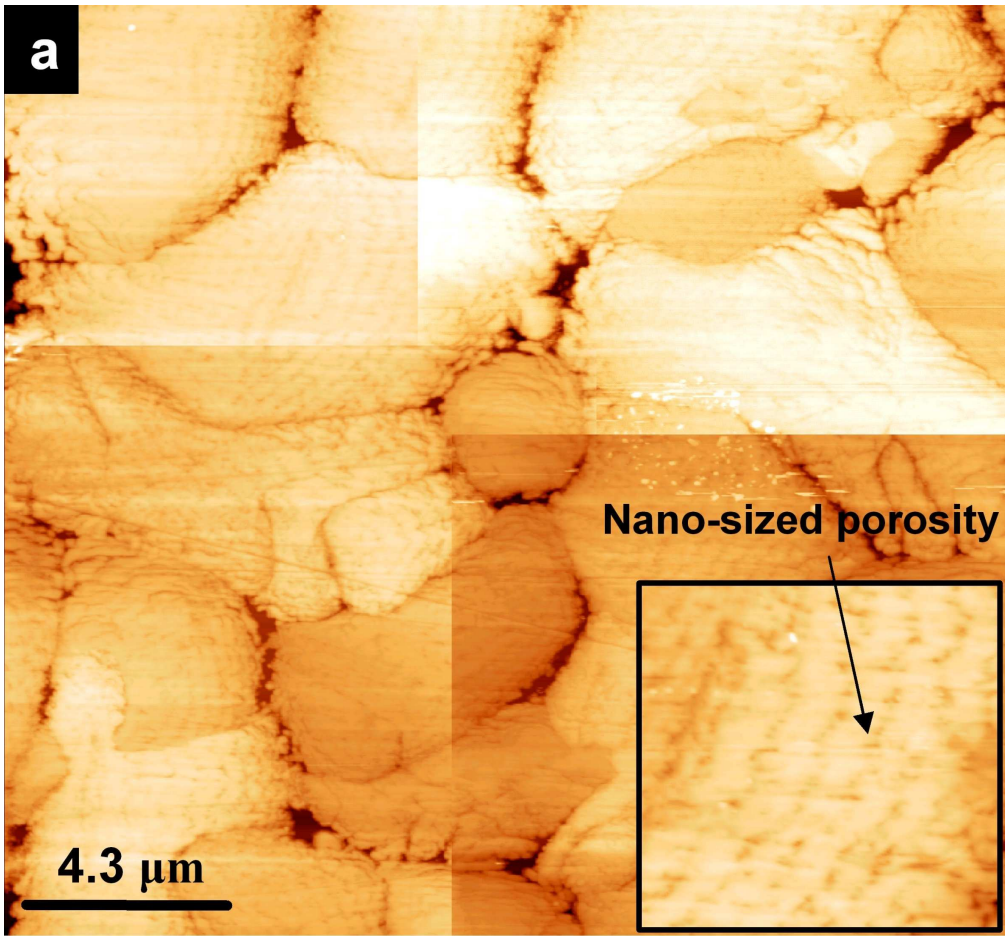

99x93mm (600 x 600 DPI)

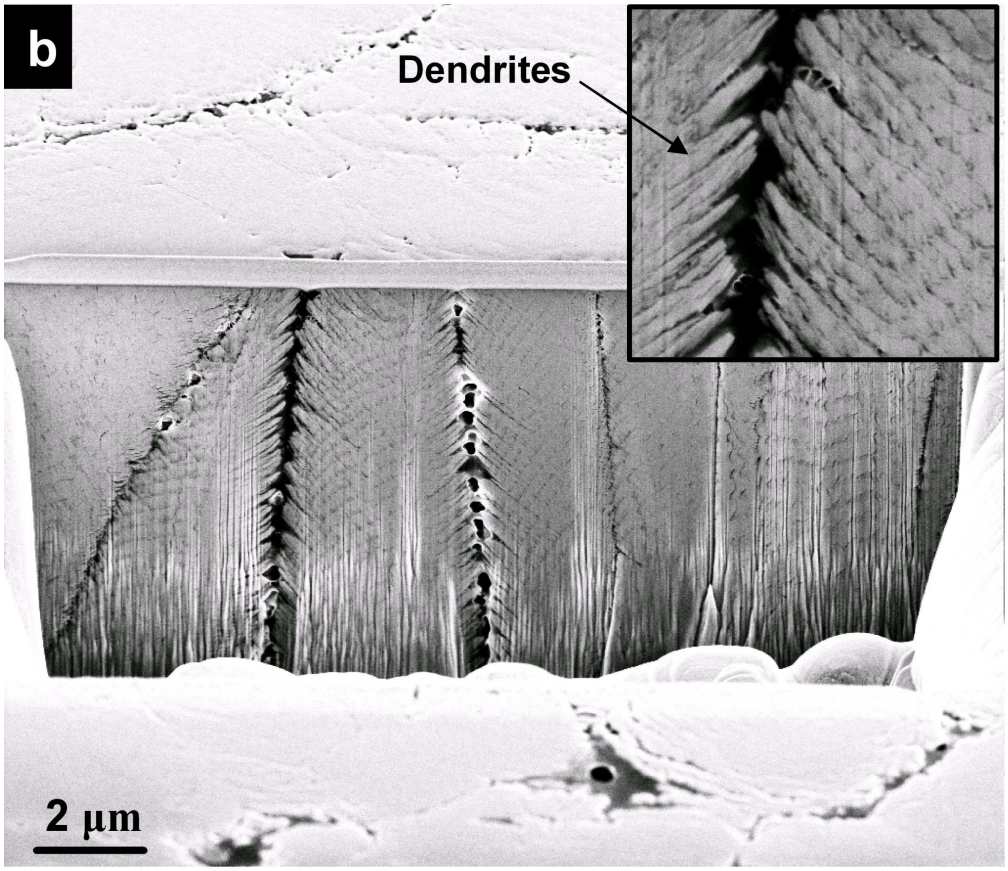

99x86mm (600 x 600 DPI)

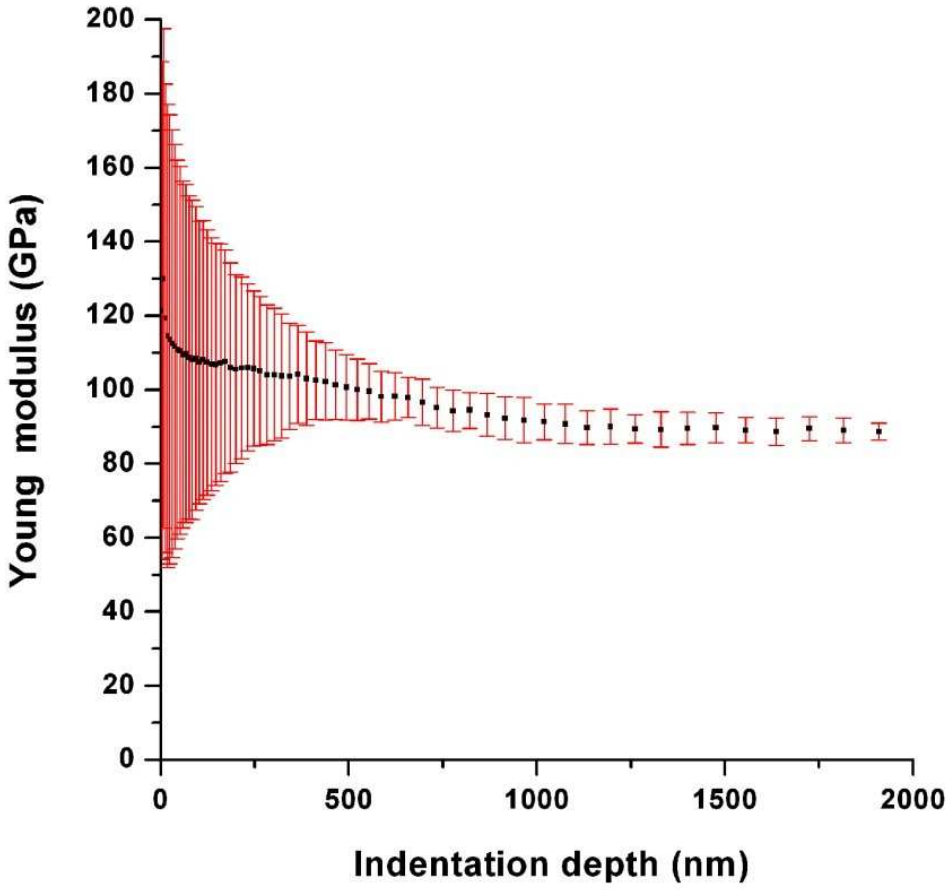

150x137mm (150 x 150 DPI)

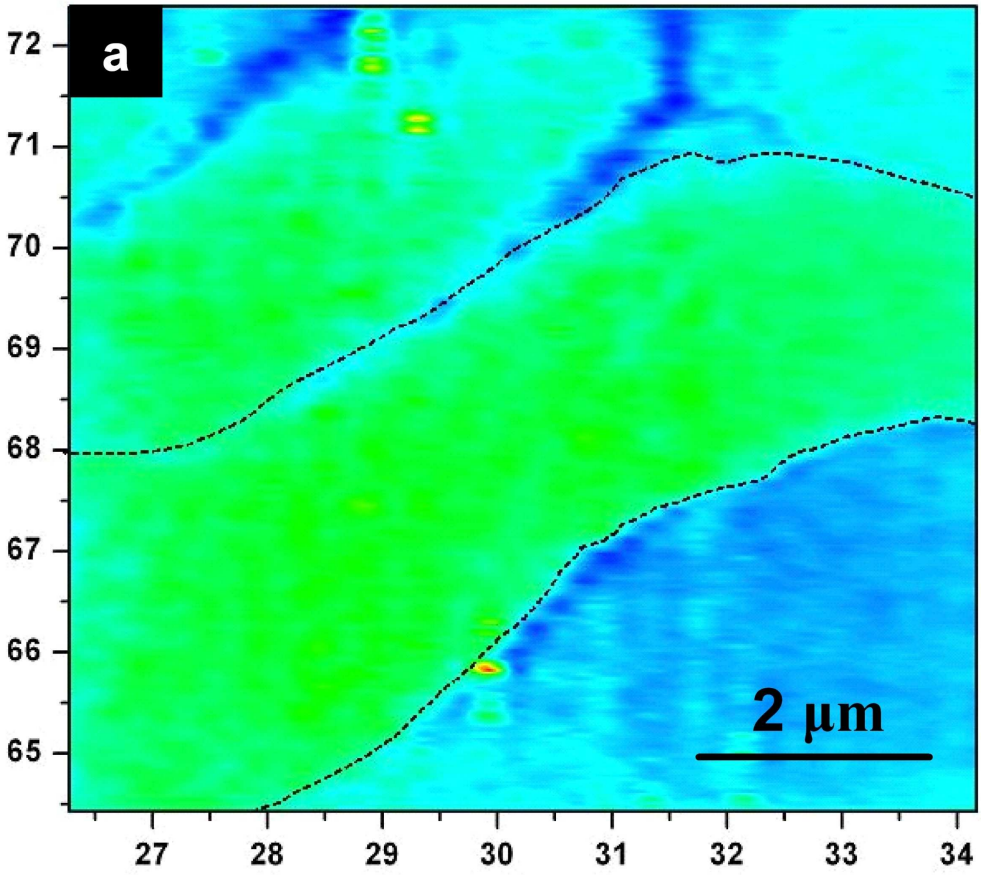

99x89mm (600 x 600 DPI)

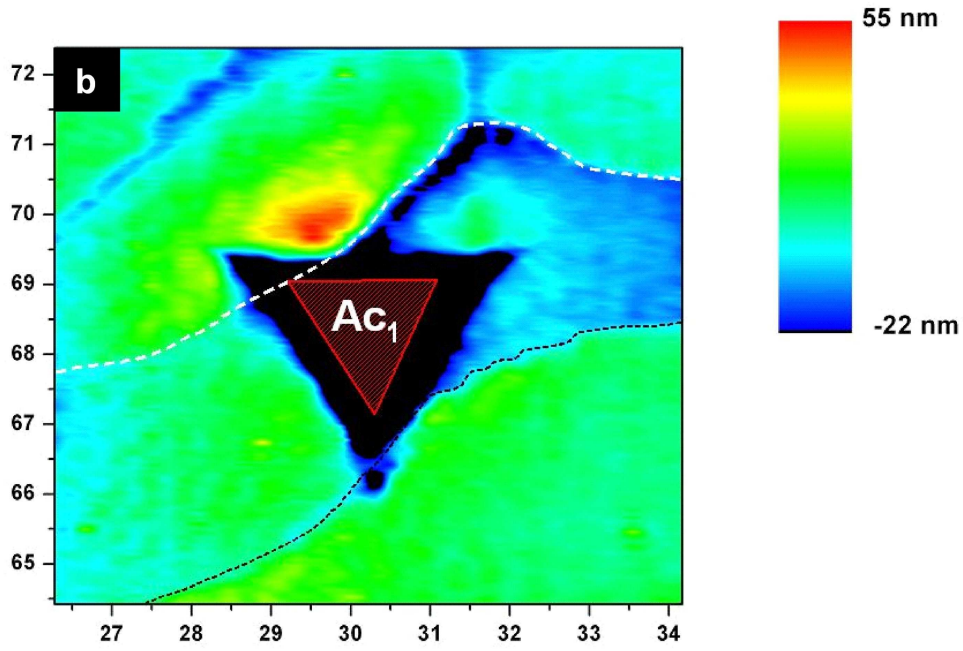

122x80mm (600 x 600 DPI)

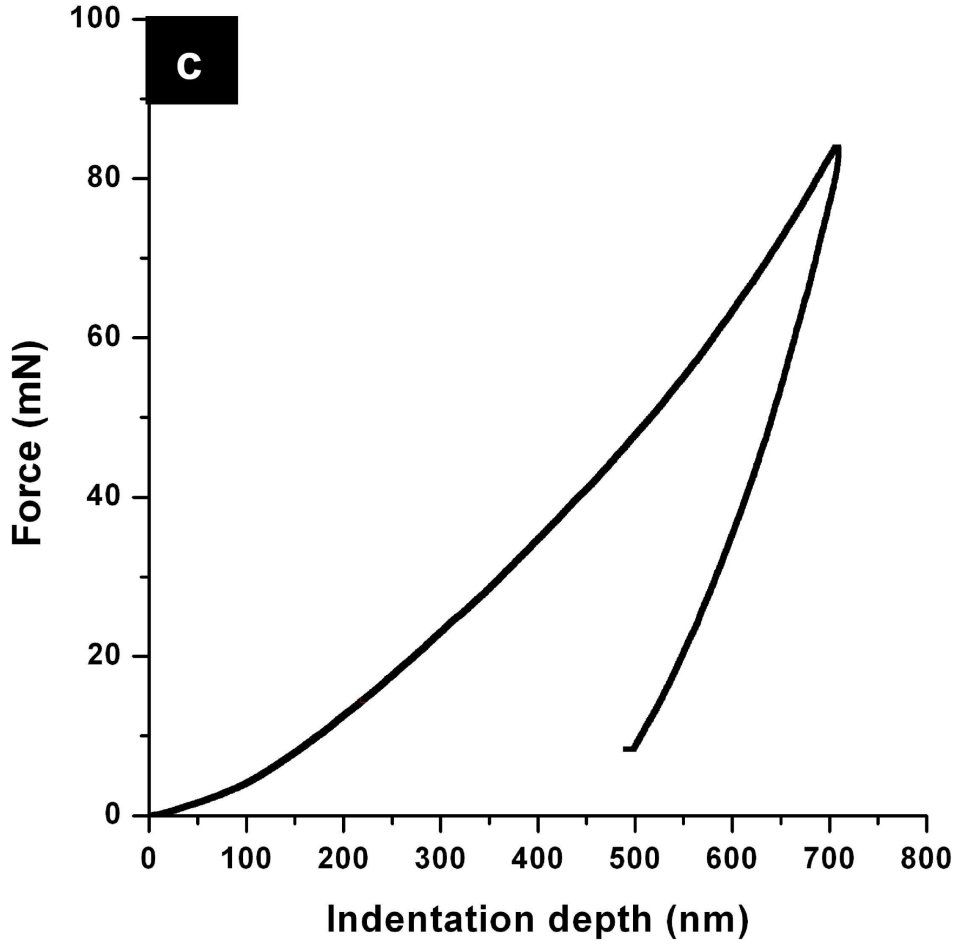

99x97mm (600 x 600 DPI)

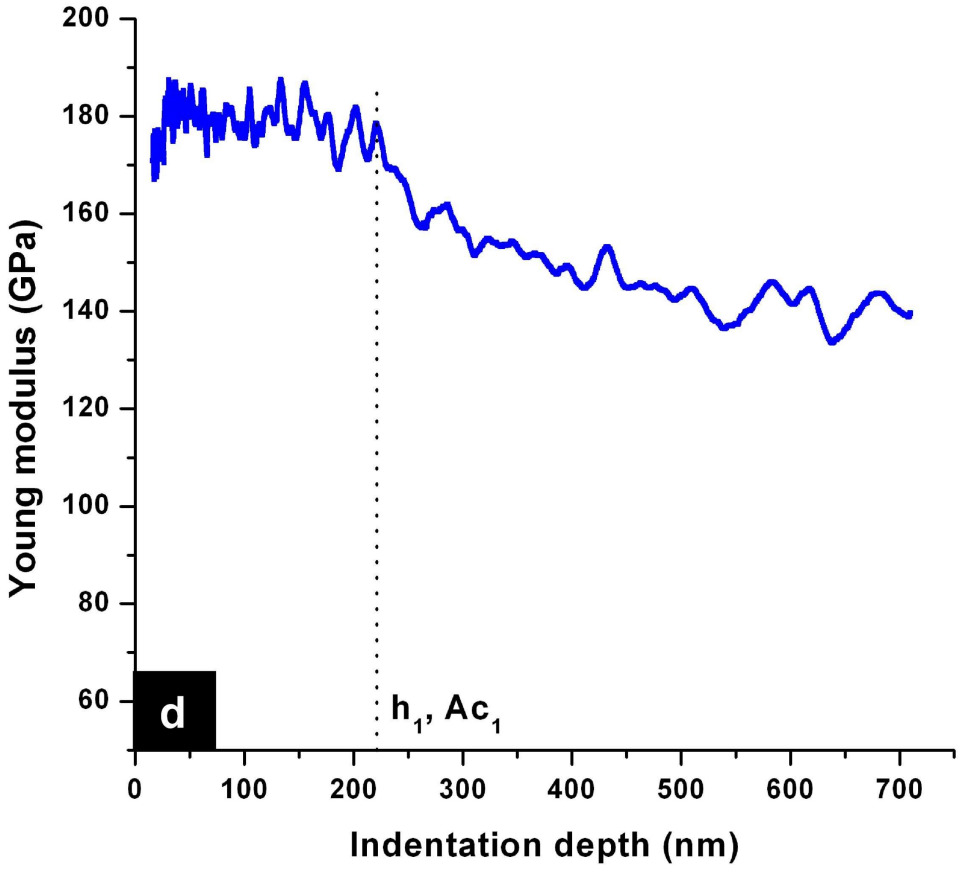

99x88mm (600 x 600 DPI)

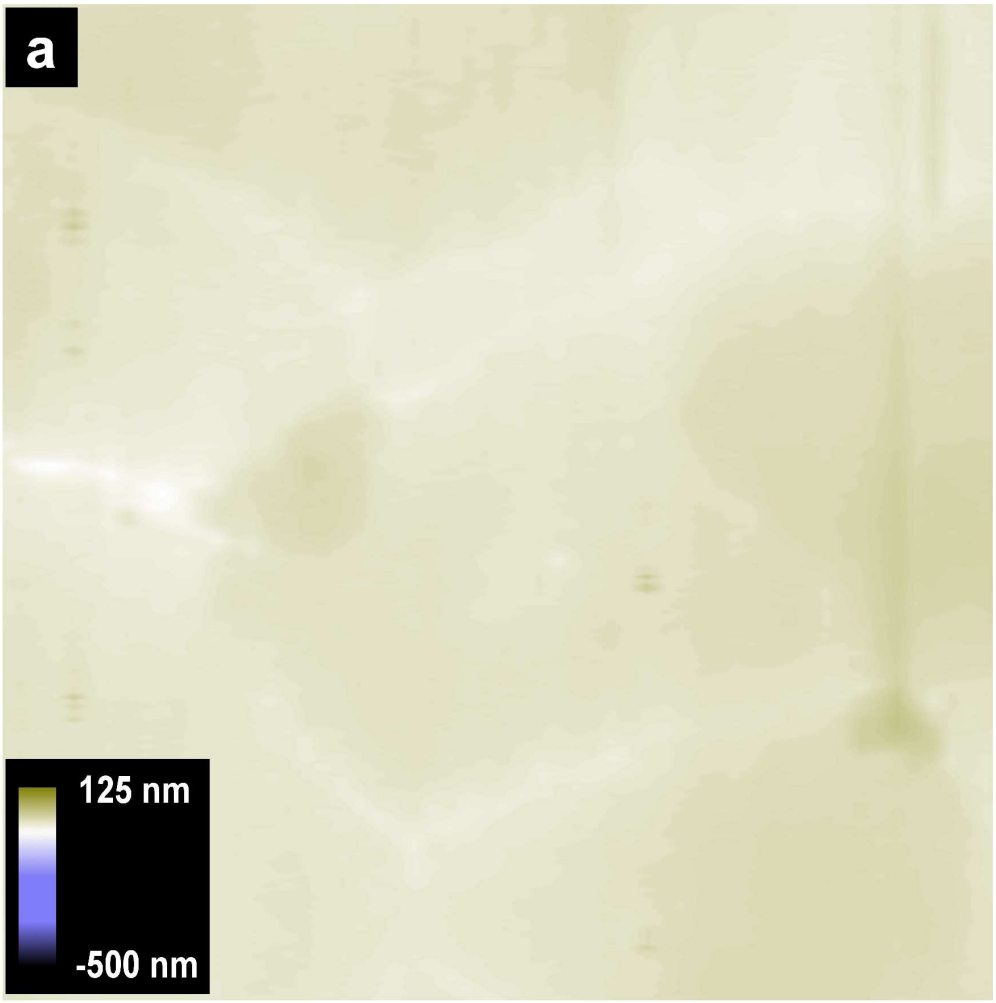

149x150mm (600 x 600 DPI)

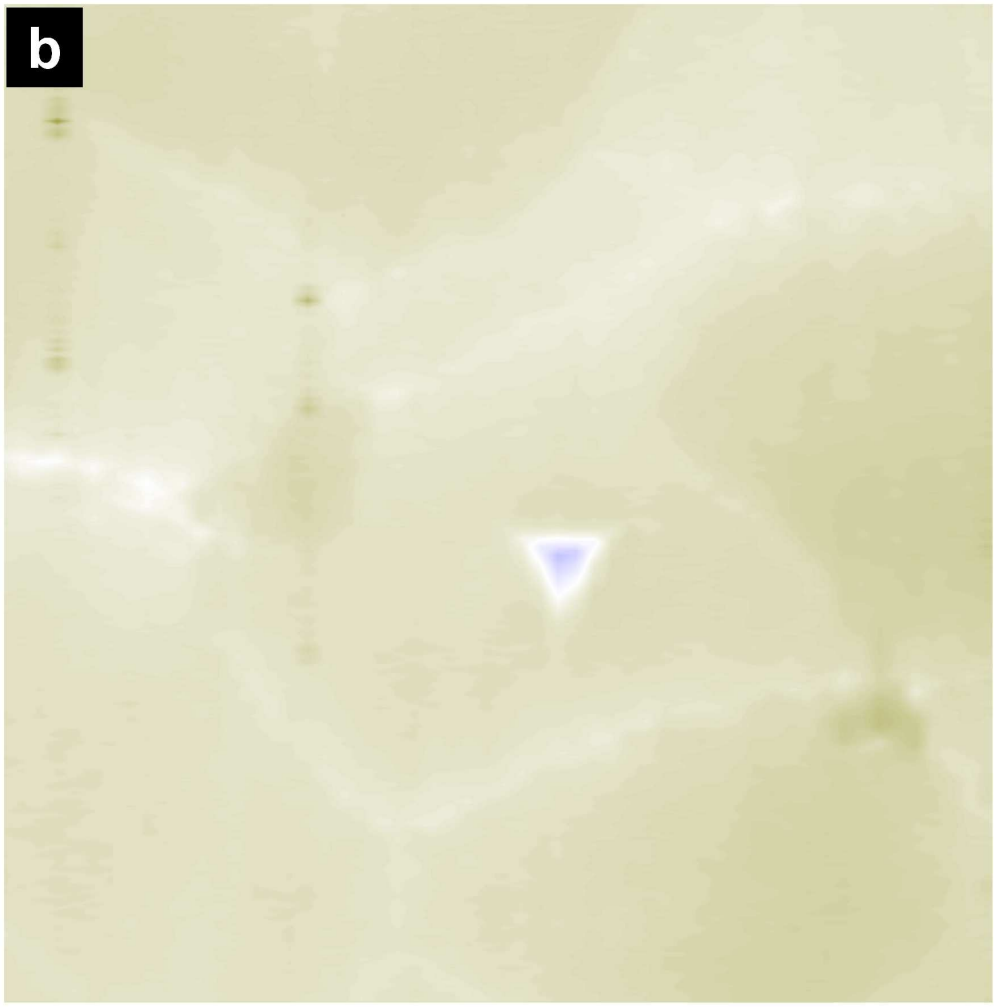

148x150mm (600 x 600 DPI)

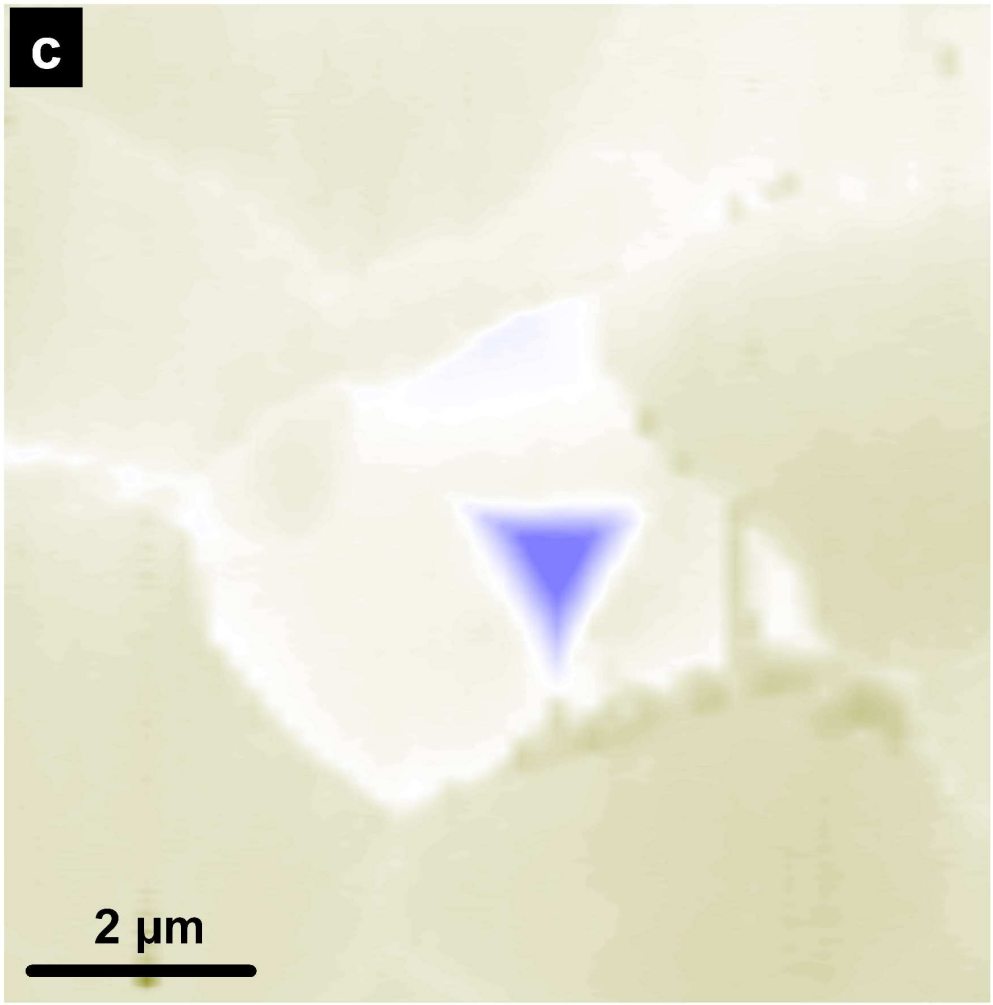

149x150mm (600 x 600 DPI)

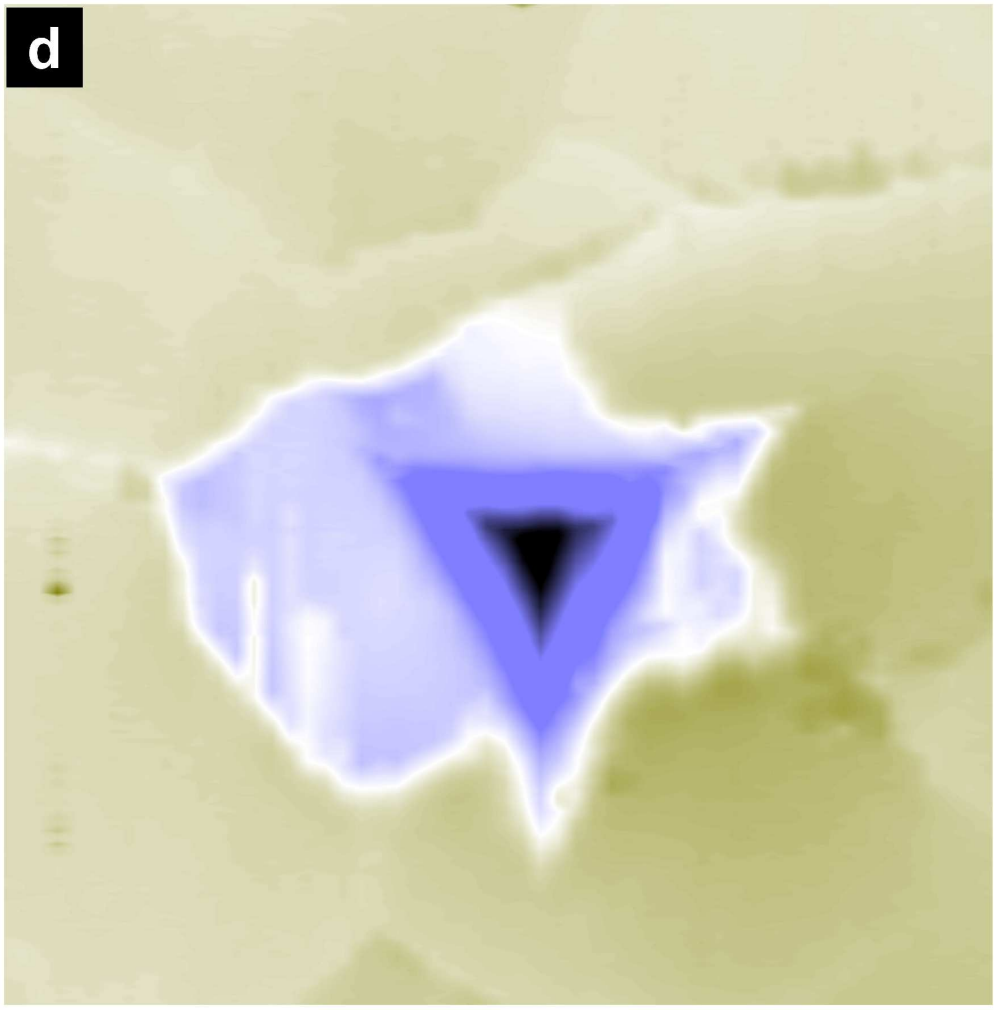

148x150mm (600 x 600 DPI)

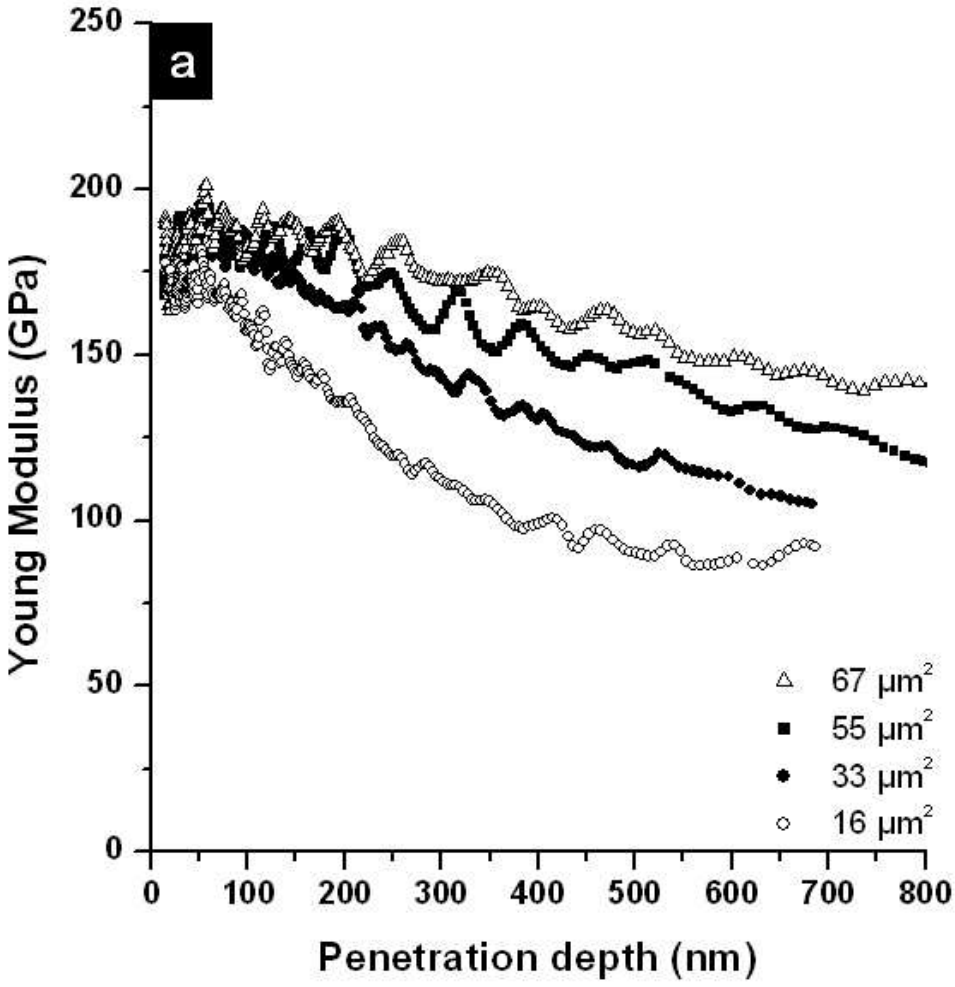
a
Young Modulus (GPa)
Penetration depth (nm)
0
50
100
150
200
250
0
100
200
300
400
500
600
700
800
67 μm²
55 μm²
33 μm²
16 μm²

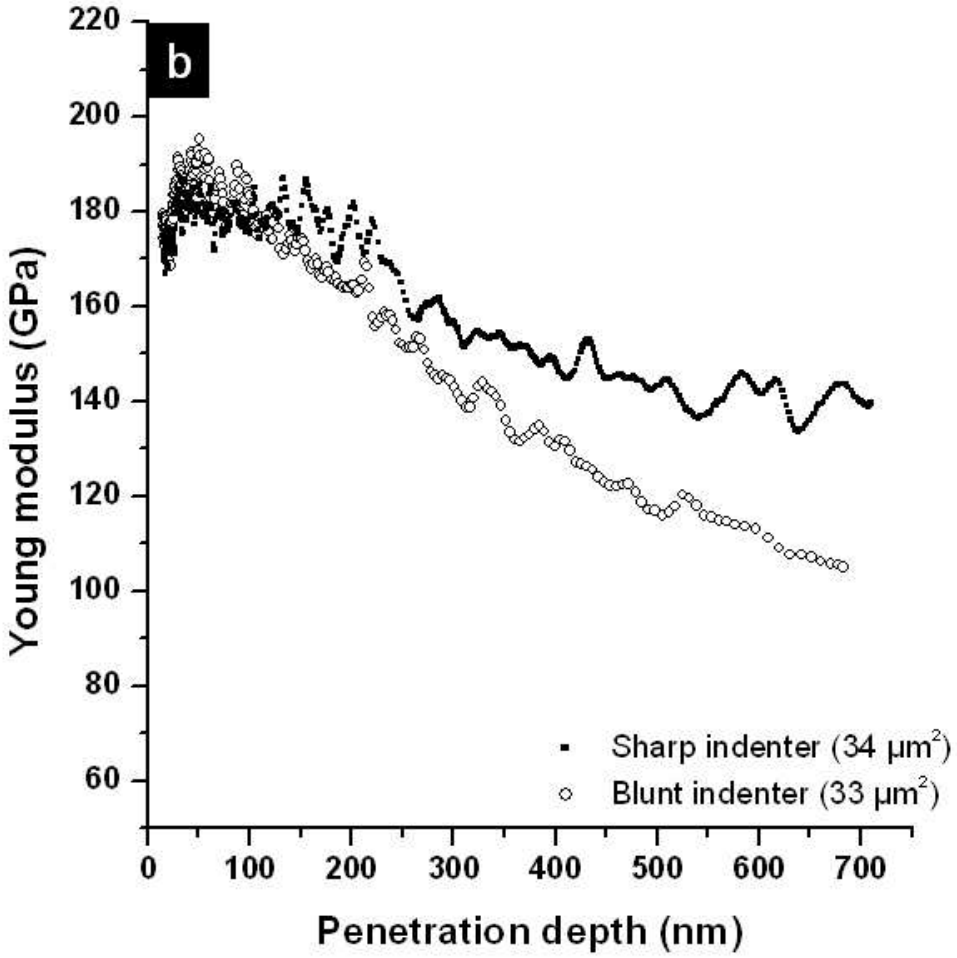
b
Young modulus (GPa)
220
200
180
160
140
120
100
80
60
0
100
200
300
400
500
600
700
Penetration depth (nm)
Sharp indenter (34 μm²)
Blunt indenter (33 μm²)

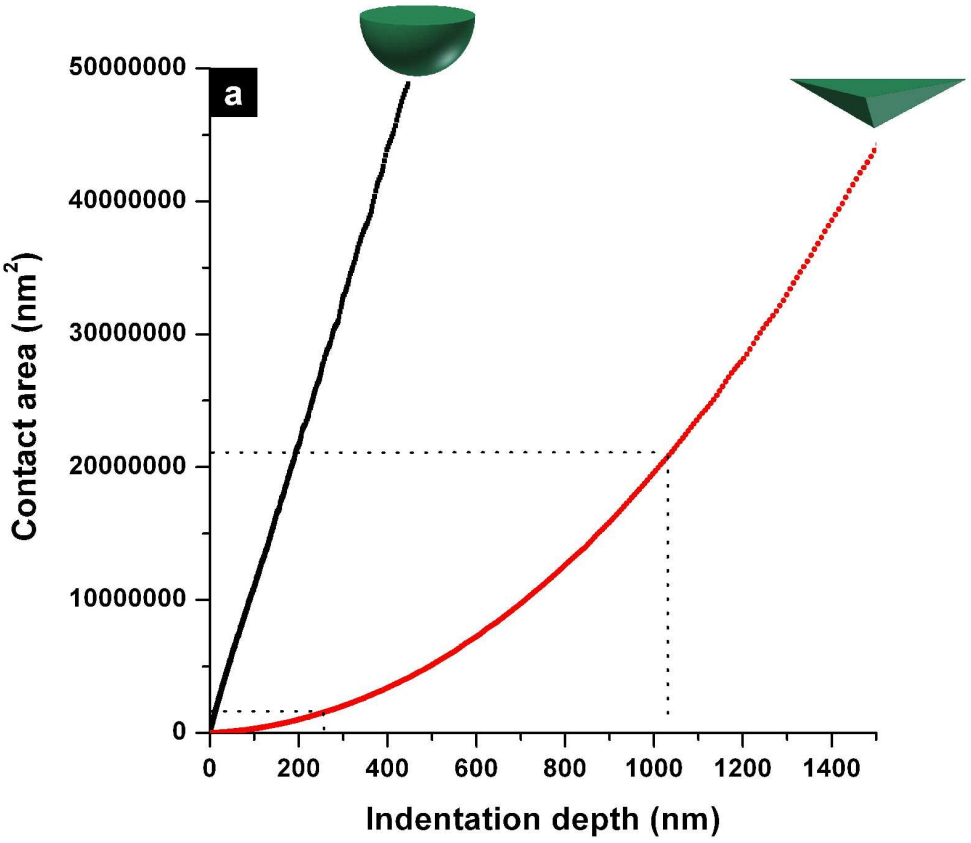

206x180mm (600 x 600 DPI)

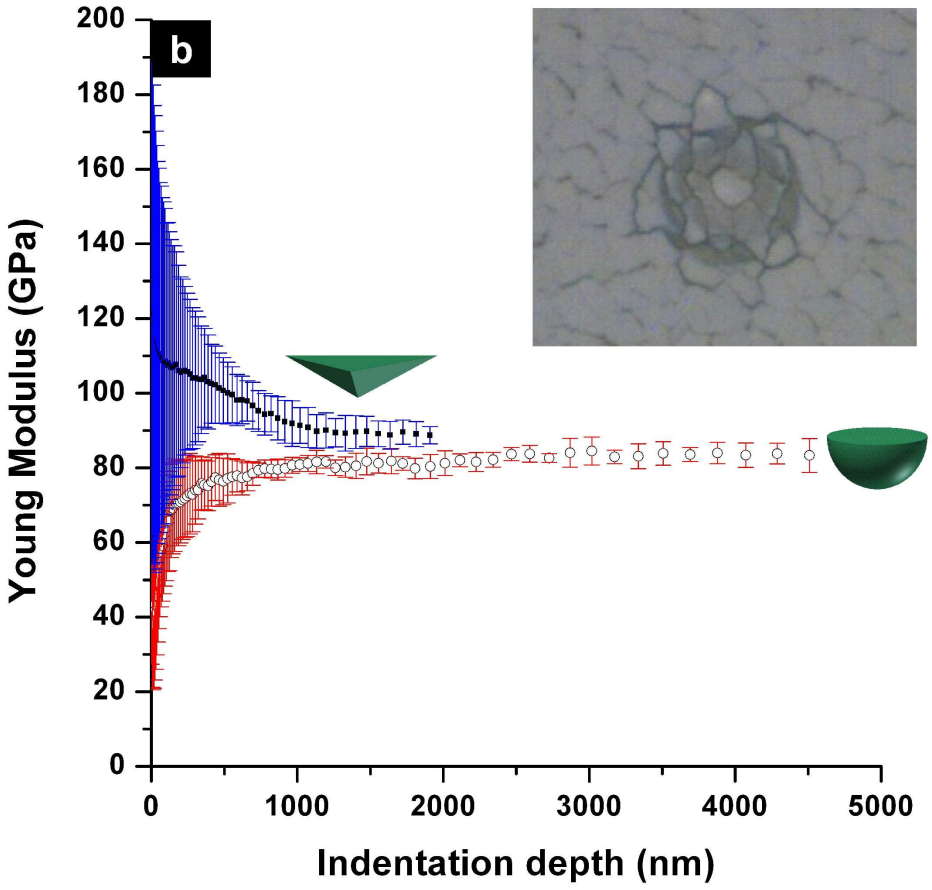

194x182mm (600 x 600 DPI)

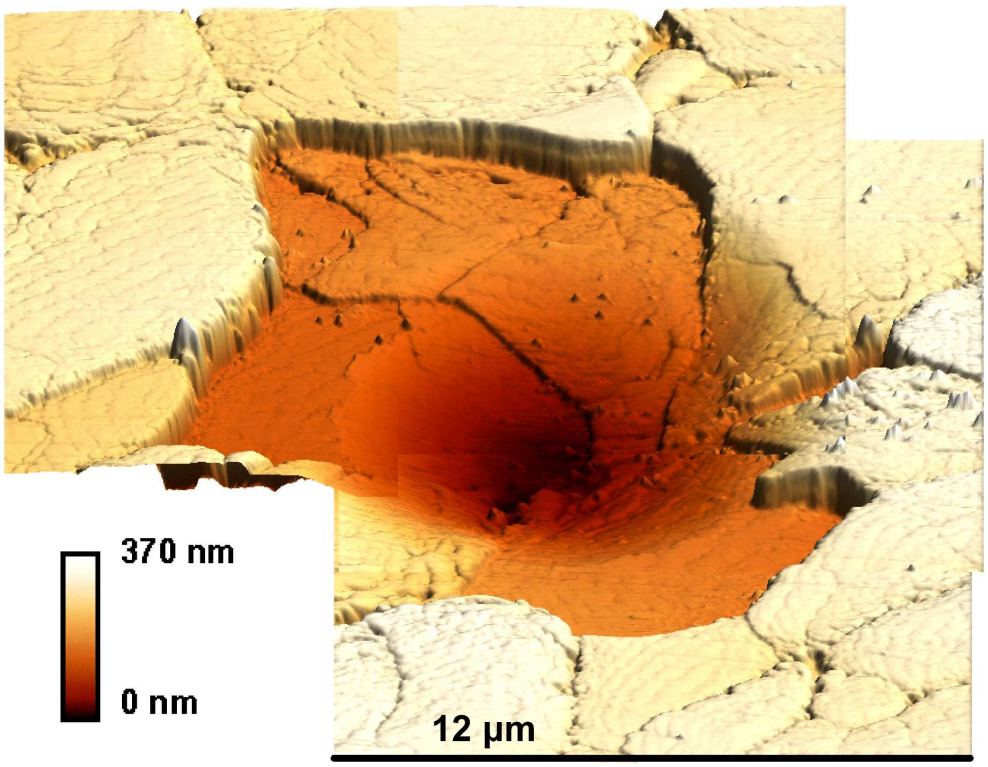

160x123mm (600 x 600 DPI)